THE WISCONSIN TORNADO OUTBREAK OF 23 JUNE 2004

Mark G. Gehring
NOAA/National Weather Service
Weather Forecast Office
Milwaukee/Sullivan, Wisconsin

Abstract

Wisconsin recorded its fifth largest tornado outbreak during the late afternoon and early evening hours of 23 June 2004. Seventeen tornadoes and numerous reports of damaging straight-line winds and large hail accompanied the complex storm structures, which consisted of bow echoes and high-precipitation (HP) supercells. One particular long-track HP supercell produced six tornadoes. One death and 23 injuries resulted from the outbreak of severe weather. Property damage totaled approximately $28.8 million, while crop damage approached $3.1 million. Although severe weather was anticipated, the number of tornadoes was somewhat unexpected. This case was characterized by fast upper flow and strong evolution of a compact surface low, resulting in rapid changes in wind shear and instability. The quick progression and evolution of the synoptic and mesoscale features, as well as relatively low dewpoints for late June, led to difficulty in identifying the magnitude of the severe threat prior to the tornado outbreak. However, analysis of observational data and Rapid Update Cycle (RUC) proximity soundings indicated the 0-1 km shear/storm-relative helicity, lifting condensation levels, and other parameters became favorable for tornadic supercells by late afternoon and evening.

Corresponding Author: Mark Gehring, NOAA/National Weather Service, N3533 Hardscrabble Road, Dousman, WI 53118 or via email: Mark.G.Gehring@noaa.gov

1. Introduction

The Wisconsin tornado outbreak during the late afternoon and evening (Galway 1977; Doswell et al. 2006) of 23 June 2004 consisted of seventeen tornadoes (Fig. 1), including four that were strong (F2 and F3 on the Fujita scale; Fujita 1971). The tornadic storms and associated

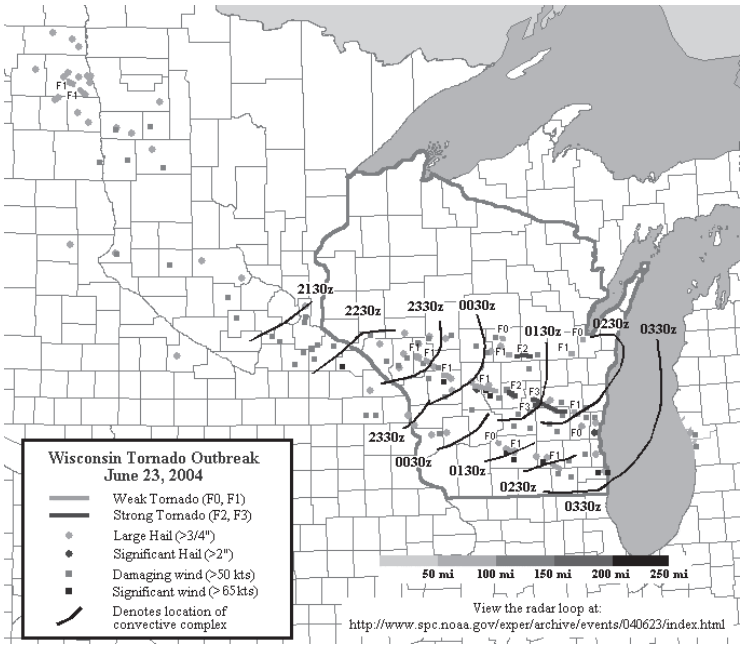

Fig. 1. Map of severe weather reports from 1430 UTC 23 June 2004 through 0425 UTC 24 June 2004.

severe hail and wind were characterized by complex storm structures, bow echoes (Fujita 1978), and supercells that were primarily of the high-precipitation (HP) variety (Moller et al. 1990). One death and 23 injuries resulted from the outbreak of severe weather.

This outbreak had only some of the "synoptically evident" parameters highlighted in other outbreaks by Doswell et al. (1993) and Johns and Doswell (1992). However, the aforementioned authors pointed out that tornado episodes can still occur in these situations, and in fact most tornado days are not "synoptically evident." As shown later, strong wind shear was in place over Wisconsin, but the surface low of approximately 1006 mb was relatively weak when compared to the "synoptically evident" tornado days. This was mainly due to the displacement of the 100 kt jet streak and strongest cyclonic vorticity advection to the north of the surface low. The displacement of the upper-level jet streak, relatively low surface dewpoints (40s°F to lower 50s°F) to begin the day, and the fast evolution/progression of the low and associated kinematic and thermodynamic fields led to difficulty in identifying the severe threat by late afternoon and evening. In the present study, the evolution of the synoptic and mesoscale environments is discussed, and close monitoring of the rapidly evolving meteorological features and severe weather indices is emphasized. Finally, the challenges faced by forecasters are briefly discussed.

2. Methodology and Data Sources

The evolution of the synoptic and mesoscale environments was analyzed from early in the day over the Northern Plains to the eventual tornado outbreak over Wisconsin in the evening. The following data sources were utilized: Rapid Update Cycle (RUC)-based mesoanalysis graphics (Bothwell et al. 2002) from the NOAA/Storm Prediction Center (SPC) Web site [available on line at www.spc.noaa.gov/exper/mesoanalysis/]; RUC-20 model (Benjamin et al. 2004) output viewed on a 40-km and 80-km grid available on the Weather Event Simulator (WES; Magsig et al. 2006); the wind profiler at Blue River, Wisconsin (BLRW3); surface observations from the Automated Surface Observing Systems (ASOS) and Automated Weather Observing Systems (AWOS); and radar images from the Weather Surveillance Radar-1988 Doppler (WSR-88D).

Severe weather parameters were calculated from six RUC analysis gridpoint soundings taken at ASOS and AWOS sites located near tornadic supercells (Fig. 2). Much research has focused on the use of proximity soundings to determine the near storm environment of tornadic versus nontornadic supercells (Markowski et al. 2003). The

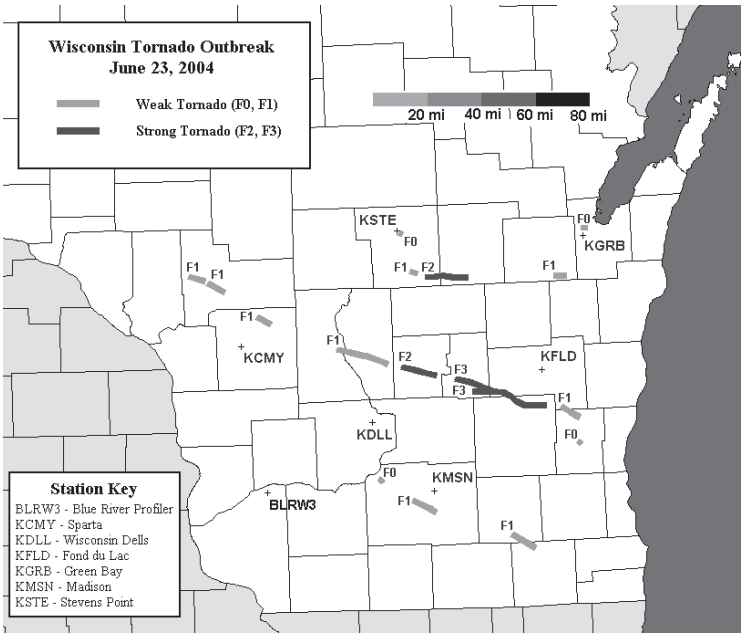

Fig. 2. Map of AWOS and ASOS locations where RUC analysis gridpoint soundings were taken. Also, Blue River profiler and tornado tracks with F-scale intensity are shown.

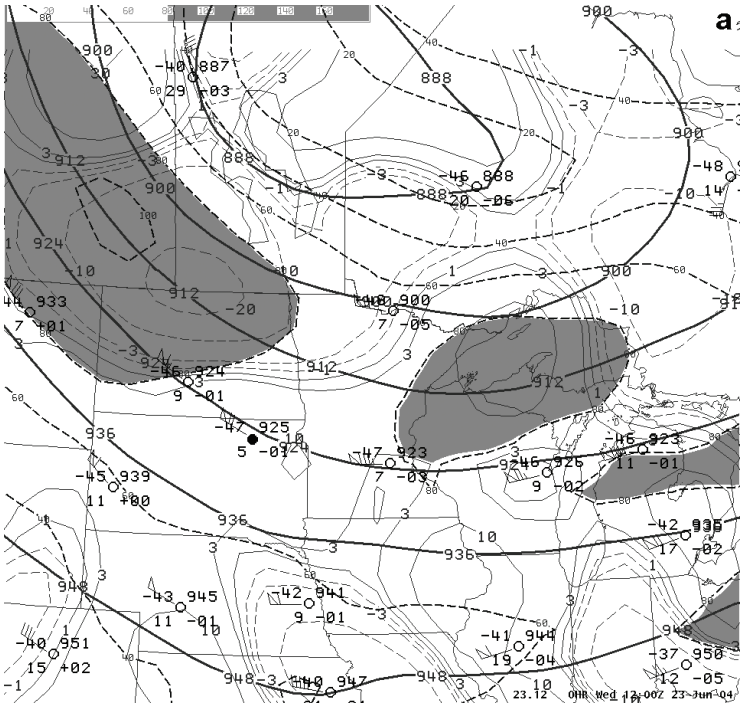

Fig. 3(a). RUC 300 mb analysis valid 1200 UTC 23 June 2004. Thick solid lines are geopotential heights every 12 dm. Black dashed lines are isotachs every 20 kt. Shading is 80 kt or greater. Thin solid gray lines are 300 mb Q-vector divergence (K m^{-2} 1e16 s^{-1}) while thin dashed lines are Q-vector convergence. RAOB data included with standard station model format.

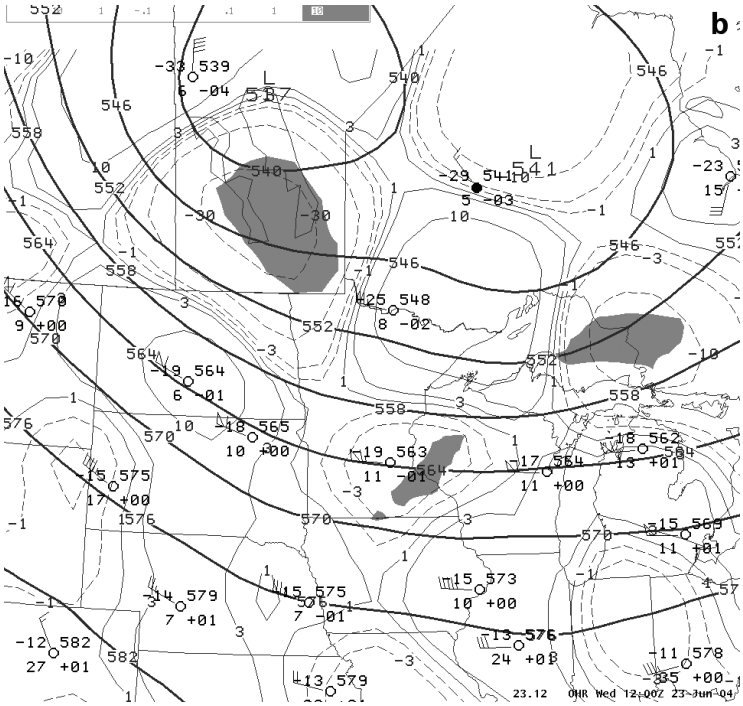

Fig. 3(b). RUC 500 mb analysis valid 1200 UTC 23 June 2004. Thick solid lines are geopotential heights every 6 dm. Thin solid gray lines are 500 mb Q-vector divergence (K m^{-2} 1e16 s^{-1}) while thin dashed lines are Q-vector convergence. Shading is 500 mb vorticity advection of 5*1e9 s^{-1} or greater. RAOB data included with standard station model format.

research by many authors has identified specific values of various parameters that favor tornadic supercells versus values that favor nontornadic supercells, and thus the findings of the proximity soundings from this tornado outbreak will be investigated. The Sounding Toolkit Version 1.5 (Bunkers et al. 2005; hereafter ST1.5), available on the WES, and a locally developed program were utilized to generate severe weather parameters for these proximity soundings. A virtual temperature correction was applied to the soundings for the analysis of thermodynamic variables (Doswell and Rasmussen 1994). There was little to no convective precipitation produced by the RUC during the time of the soundings; hence, no contamination from the convective parameterization scheme occurred.

3. Synoptic and Mesoscale Setting and Evolution

a. 1200 UTC to 2100 UTC

The upper air features (Fig. 3a-c) were dominated by a broad and cold cyclonic circulation centered over Manitoba and Ontario. A 300-mb (100 kt) jet and a 500-mb shortwave trough were digging southeast toward the Dakotas, with cold 500-mb temperatures from -16°C to -19°C already located over Wisconsin. Warm-air advection (5°C per 12 hour) was evident at 850 mb over northeastern North Dakota and northwestern Minnesota (not shown). At the surface (Fig. 3d), a cold front extended west from a 1010 mb open wave of low pressure over southeastern Manitoba, with a surface trough extending south of the low. Deep (low and mid levels) Q-vector convergence was evident with these synoptic features over eastern North Dakota and northwestern Minnesota. Stronger upper-level Q-vector convergence was maximized upstream over southern Manitoba, where the left exit region and greatest 500 mb cyclonic vorticity advection was located. Farther east, a surface cold front extended from eastern Lake Superior to northern Iowa. Surface dewpoints ranged from the 40s (°F) to the lower 50s (°F) across Minnesota and Wisconsin with areas of middle 50s (°F) dewpoints near and south of the cold front. The cold front was expected to stall with sufficient moisture and heating anticipated along and south of the front for surface-based convective initiation later in the day. This synoptic setup which included increasing vertical wind shear allowed forecasters to anticipate severe thunderstorms but not necessarily a tornado outbreak. More on the challenges of the forecast will be discussed in Section 4.

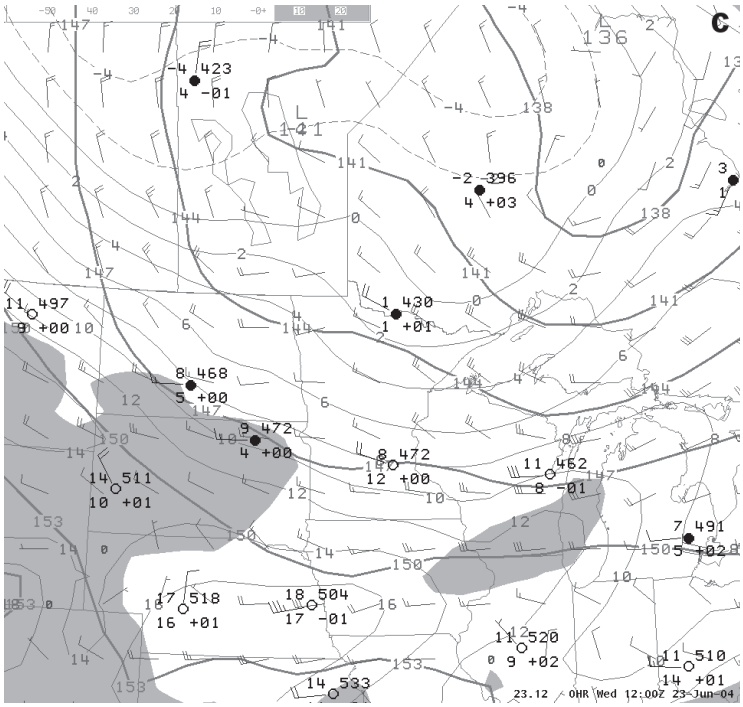

Fig. 3(c). RUC 850 mb analysis valid 1200 UTC 23 June 2004. Thick solid lines are geopotential heights every 3 dm. Thin solid lines are temperature every 2°C. Shading are dewpoints of 4°C or greater. RUC wind barbs (kt) included and RAOB data included with standard station model format.

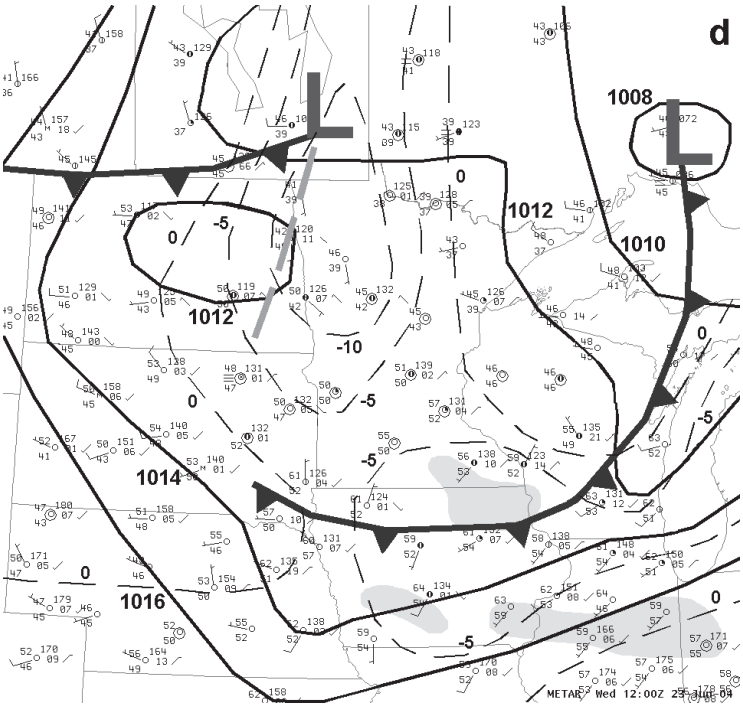

Fig. 3(d). Subjective surface analysis valid 1200 UTC 23 June 2004. Black dashed lines are RUC analysis 1000-850 mb Q-vector convergence (K m^{-2} 1e16 s^{-1}). Solid lines are isobars contoured every 2 mb. Long and thick dashed line is a surface trough. Solid symbols are conventional surface features. Standard station model format are shown. Shading represents dewpoints of 55°F or greater.

Despite very low mean-layer (ML; Craven et al. 2002) convective available potential energy (MLCAPE) around 100 J kg^{-1} (not shown) within the small warm sector over far eastern North Dakota and far northwestern Minnesota, organized convection developed by mid-morning as the Canadian cold front and aforementioned Q-vector convergence progressed across the region. The convection produced two weak (F0 and F1 on the Fujita scale) tornadoes (Fig. 1). Boundary layer-6 km shear (not shown) from 50 to 60 kt was prevalent across the Northern Plains into northwestern Wisconsin. This strong deep layer shear is supportive of supercell storms (Weisman and Klemp 1982, 1984). Johns et al. (1993) found that tornadic supercells can occur in environments with very low MLCAPE and strong shear. The low instability and high wind shear environment was prevalent throughout this event.

By 1800 UTC, the cold front had moved across northwestern Minnesota and extended west into the Dakotas (Fig. 4a). A warm front extended southeastward across Minnesota into northern Illinois where it joined with a stationary front, previously a cold front, Fig. 3d. A north to south surface trough had developed in the warm sector over southwestern Minnesota. The earlier convection was still ongoing along the cold front as seen in the 1815 UTC visible satellite image (Fig. 5a). Meanwhile a new area of deep moist convection had developed just to the south near the intersection of the surface trough and cold front in west-central Minnesota. The new convection initiated in a narrow axis of MLCAPE (600 J kg^{-1}) with much lower MLCAPE present to the east across Minnesota (not shown).

The 1800 UTC wind fields (compared to 1200 UTC) had increased within the warm sector and behind the cold front. This was in response to dynamically induced isallobaric couplet that had developed across western Minnesota and North Dakota (Fig. 4a). The increased pressure gradient and low-level wind fields resulted in frontogenesis (Fig. 6) along the cold front, along with an increase in warm-air advection, 1000 mb-850 mb equivalent potential temperature (theta-e) advection, and the associated Q-vector convergence (Fig. 7a) across most of Minnesota. These processes, along with strong insolation within the warm sector, were important factors in providing moisture, instability, and lift (Doswell 1987) to developing convection as it moved east across southern Minnesota during the afternoon. The deep moist convection that initiated near the surface trough and cold front intersection progressed eastward across southern Minnesota (Fig. 5b) and did result in isolated to scattered severe hail and wind reports (Fig. 1). The convection

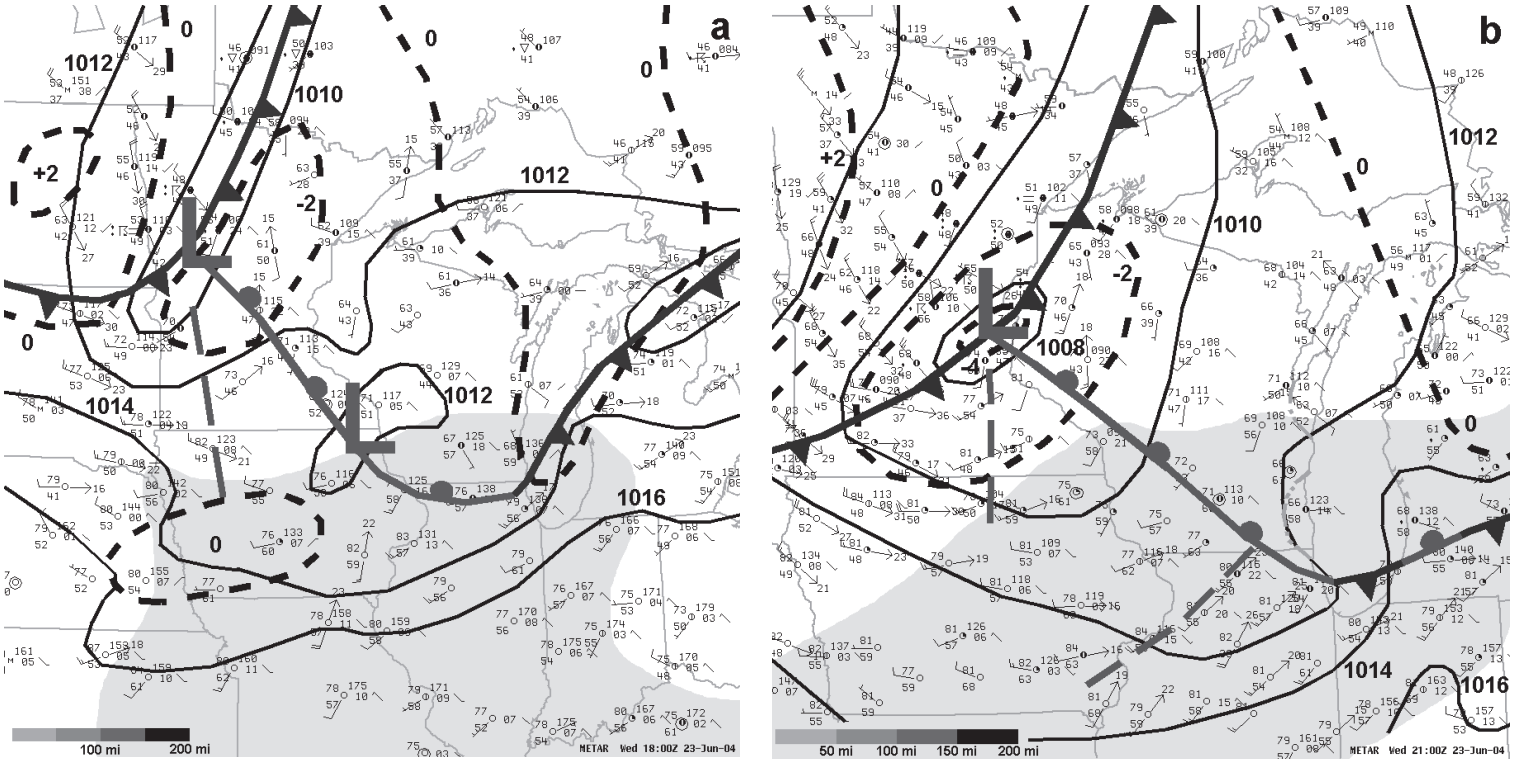

Fig. 4a-d. Subjective surface analysis for (a) 1800 UTC, (b) 2100 UTC, (c) 0000 UTC, (d) 0300 UTC. Solid lines are isobars contoured every 2 mb. Long dashed lines are surface troughs. Short dashed lines are 3-hour pressure change contoured every 2 mb. Solid symbols are conventional surface features. Standard station model format is shown. Shading represents dewpoints of 55°F or greater.

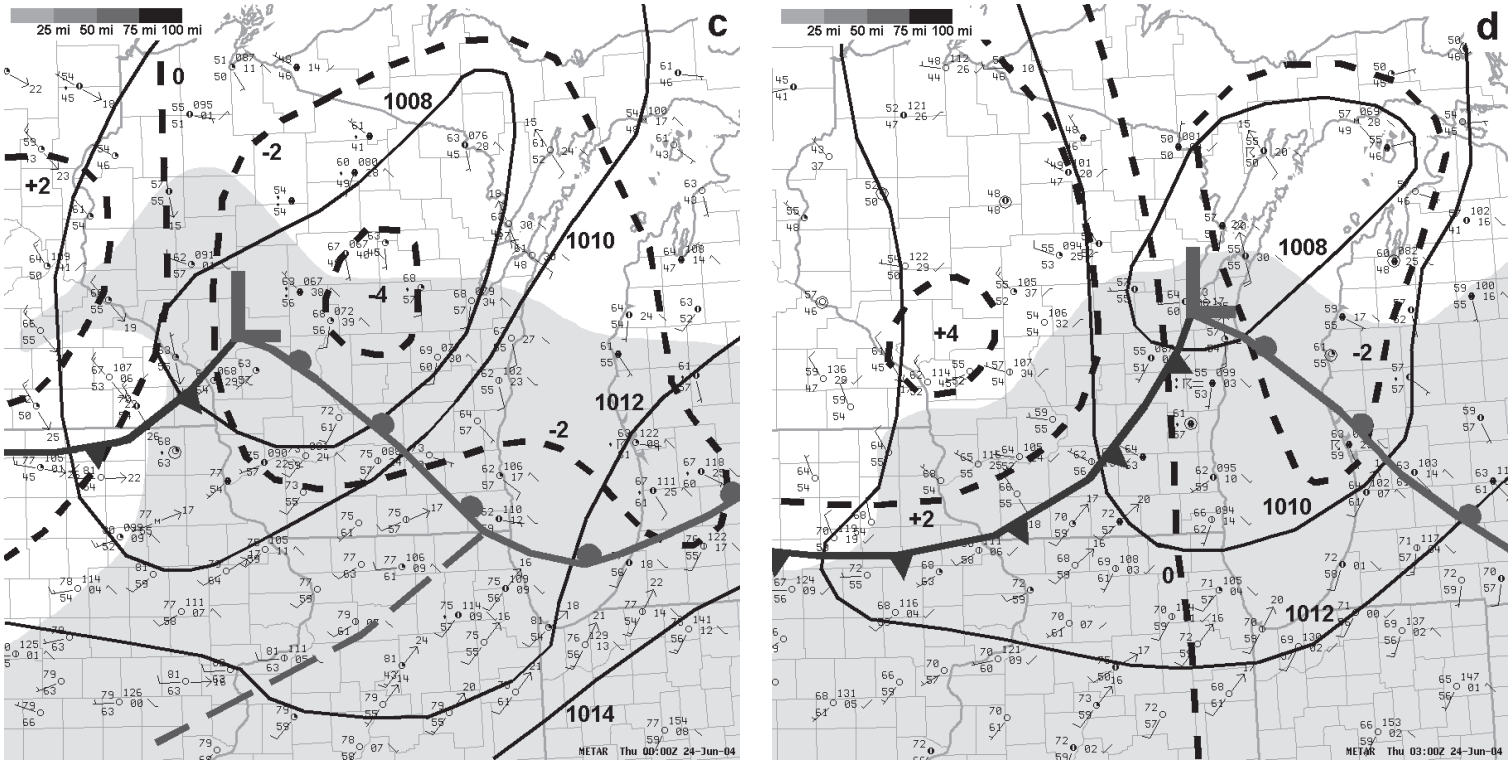

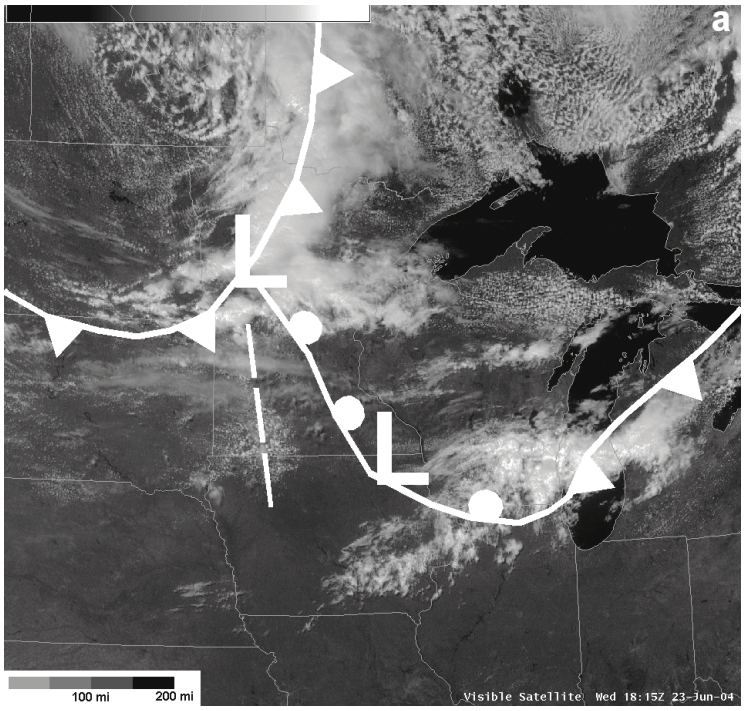

Fig. 5(a). Visible satellite image for 1815 UTC. Solid symbols are conventional surface features.

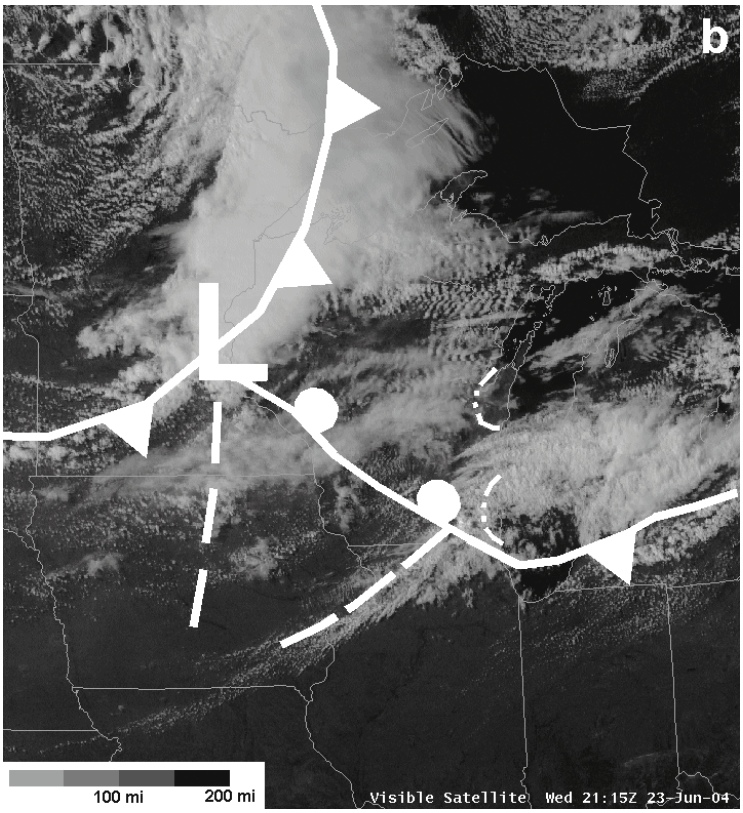

Fig. 5(b). 2115 UTC.

would eventually evolve into a significant severe convective complex across Wisconsin. The convection to the north also translated eastward but remained north of a developing surface low without any further severe weather.

Also at 1800 UTC and farther to the southeast, an area of subsynoptic low pressure had formed over northeastern Iowa along the stationary front (Fig. 4a). This low may have been a surface reflection of a low amplitude shortwave trough at 500 mb (Fig. 3b). The resultant pressure gradient allowed southwest winds to prevail along and south of the stationary front while lighter winds and high-based scattered showers and isolated thunderstorms existed north of the front over southern Wisconsin (Fig. 5a). This acted to maintain weak frontogenesis (Fig. 6) and surface moisture flux convergence (not shown) along and north of the stationary front.

By 2100 UTC, a closed surface low had developed near Minneapolis (Fig. 4b). The isallobaric couplet shifted southeastward into most of Minnesota and the low had deepened 3.5 mb since 1800 UTC. The warm front and trailing surface trough had surged eastward and extended south-southeast of the low. The surface analysis and 2115 UTC visible satellite image (Fig. 5b) showed a band of towering cumulus with WSR-88Ds detecting scattered showers (not shown) along the surface trough. Surface dewpoints were mainly in the 40s (°F) along and west of the warm front and surface trough over Minnesota. The minimal surface moisture (very low MLCAPE) and

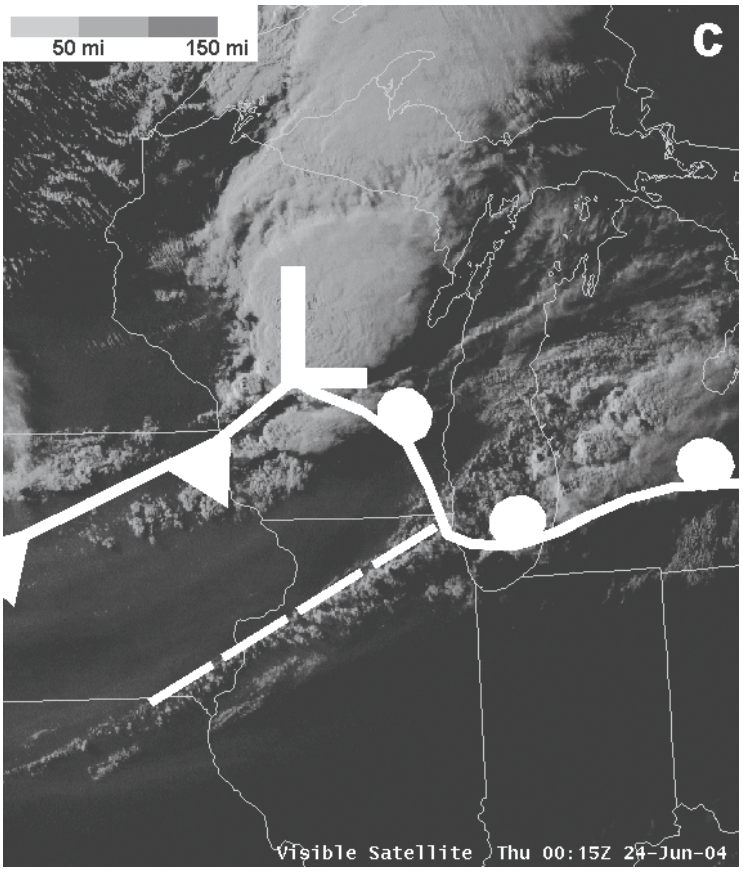

Fig. 5(c). 0015 UTC.

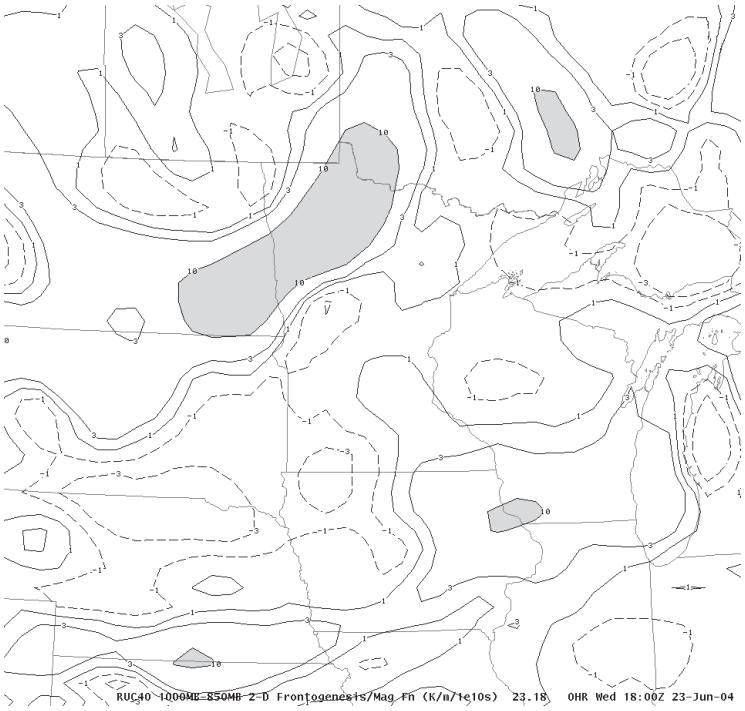

Fig. 6. 1800 UTC RUC 1000-850 mb two-dimensional frontogenesis (K m^{-1} 1e10 s^{-1}) analysis. Shading is 10 K m^{-1} 1e10 s^{-1} or greater.

southward displacement from the upper-level dynamics appeared to be limiting factors for deep, severe convection across southern Minnesota. However, this was not the case farther north across east-central Minnesota, near the surface low and cold front. A bow echo and other isolated convection were evident northwest of Minneapolis at 2040 UTC (not shown). The bow echo dissipated shortly thereafter, but new cells developed ahead of and along an associated gust front. Although this severe weather event did not qualify as a "northwest flow outbreak" (Johns 1982; average 500 mb flow was not 280 degrees or greater), the surface pattern at 2100 UTC (Fig. 4b) and throughout this event resembled type "Q2" in Johns (1984). Type "Q2" convection occurs in the vicinity of the surface low and the upper levels are defined by a digging shortwave trough. For this event, severe deep moist convection occurred near the surface low and in the vicinity of the fronts and trough lines. However, the strong 500-mb shortwave trough and jet streak remained mostly across northern Minnesota and Lake Superior during the afternoon and evening. The surface low through 2100 UTC was on the southern periphery of Q-vector convergence (not shown) from 700 mb up to 300 mb, implying the aforementioned upper dynamics contributed to the deepening of the surface low. The northward displacement of the left exit region, 500 mb cyclonic vorticity advection, and the associated upper level Q-vector convergence is discussed in more depth later in this paper.

Over central Wisconsin, south winds had developed in response to the isallobaric couplet. Low-level moisture began to advect northward into central Wisconsin (Fig. 7b) and dewpoints increased 3-7 (°F) between 1200 UTC and 1800 UTC (Fig. 4b). The surface-based CAPE at 2200 UTC was from 500 to 1000 J kg^{-1} to the east-southeast of the surface low (Fig. 8). But over southern Wisconsin, less cloud cover and therefore strong insolation had resulted in surface-based CAPE from 1500 to 2000 J kg^{-1}. Convergence along a lake breeze front (Fig. 5b) and along a southwest-to-northeast oriented surface trough (Fig. 4b) initiated surface-based convection in far southeastern Wisconsin around 2100 UTC (Fig. 5b). New convection developed south along the surface trough through 2200 UTC. The thunderstorms did become severe in far southeastern Wisconsin for a short time before moving eastward into Lower Michigan.

b. 2100 UTC to 0300 UTC

Between 2100 UTC and 0300 UTC, the surface low and isallobaric couplet progressed from Minneapolis to Green Bay without any further deepening of the low (Fig. 4b-d). The warm front from Minneapolis to far southern Wisconsin lifted to the northeast, continuing the advection of low-level moisture into central Wisconsin. The cold front translated well into southern Wisconsin by 0300 UTC. Early during this period, new thunderstorms developed along the surface trough over far southeastern Minnesota as it pushed into a higher CAPE environment (Fig. 8). This new area of thunderstorms and the ongoing thunderstorms near Minneapolis evolved into a severe convective complex of mostly HP supercells and bow echoes as it tracked across central and southern Wisconsin (Fig. 5c). Figure 9 displays several of the HP supercells from various WSR-88Ds at 0.5 elevation reflectivity.

The strong deep layer wind shear that was already in place across the Northern Plains into northwestern Wisconsin had expanded eastward over the western Great Lakes by 1800 UTC. The bulk Richardson number (BRN; Weisman and Klemp 1982) shear was consistently 80 m^2 s^{-2} or larger throughout this event (Fig. 8). This is well into the range of tornadic supercell storms (Thompson 1998; Thompson et al. 2003, hereafter T03). While strong deep-layer shear was in place throughout this event, the low-level wind shear attained an appreciable increase from the late afternoon into the evening hours. This was due to the isallobaric couplet and the resultant increase in the pressure gradient east and south of the surface low (Fig. 4c). The increase in wind speed is shown by the Blue River, Wisconsin wind profiler (Fig. 10). The most substantial increase in wind speed around 15 kts occurred within the 0-2 km layer between 2100 UTC and 0000 UTC. The following parameters also indicated an increase in low-level

wind shear between 2200 UTC and 0100 UTC: surface-1 km shear (Fig 11a-b), 0-3 km storm-relative helicity (SRH; Davies-Jones et al 1990; Fig. 12a-b), and 0-1 km SRH (Fig. 12c-d). Surface-1 km shear increased sharply from less than 10 kt to 15 to 25 kt by 0100 UTC. Craven et al. (2004) revealed that 0-1 km shear discriminates very well between significant tornadoes and other severe events. Their data suggested a lower general guideline of 10 m s^{-1} may be used for significant tornadoes.

The 0-3 km SRH and 0-1 km SRH [using the Bunkers et al. (2000) supercell motion estimate] had maximum values around 200 m^2 s^{-2} and 100 m^2 s^{-2} respectively in the vicinity

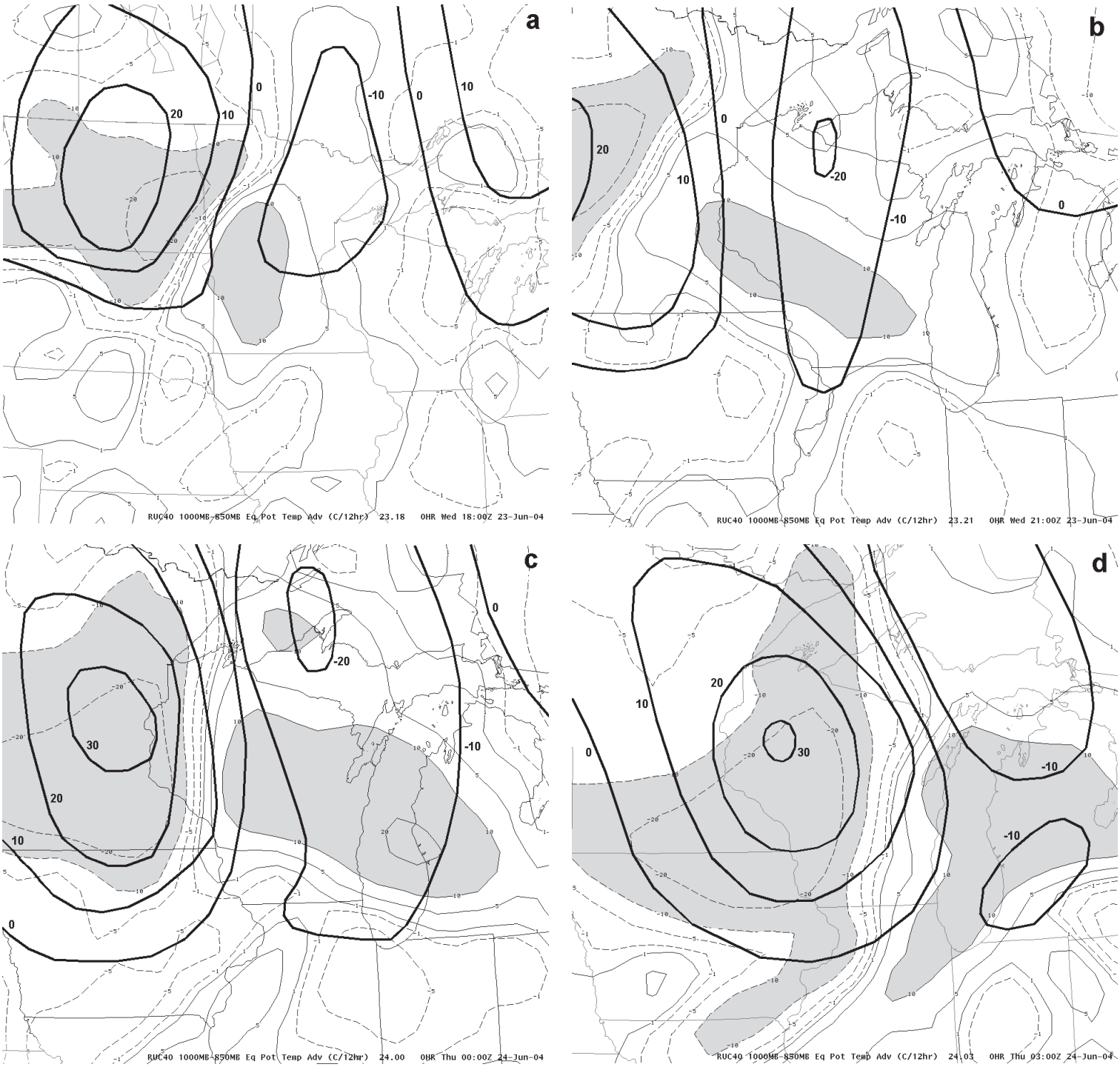

Fig. 7 (a-d). RUC 1000-850 mb equivalent potential temperature advection (C 12 hr^{-1}) analysis and 1000-850 mb positive and negative Q-vector divergence for (a) 1800 UTC, (b) 2100 UTC, (c) 0000 UTC, and (d) 0300 UTC. Thin solid and dashed gray lines are theta-e advection with shading for 10 C 12 hr^{-1} or greater and -10 C 12 hr^{-1} or less. Solid black lines are 1000-850 mb positive and negative Q-vector divergence (K m^{-2} 1e16 s^{-1}).

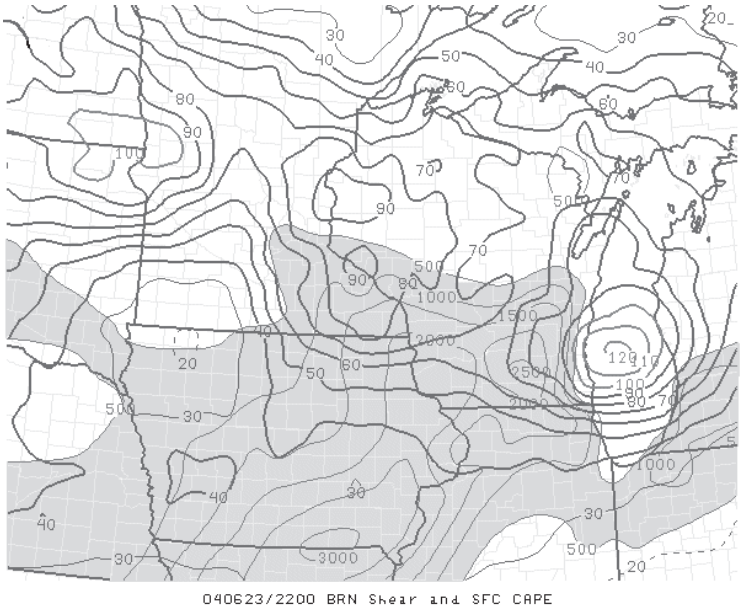

Fig. 8. SPC RUC-based BRN shear and surface CAPE valid 2200 UTC 23 June 2004. CAPE greater than 500 J kg^{-1} is shaded.

of the convective complex over southeastern Minnesota and far western Wisconsin. Another maximum was located over far southeastern Wisconsin and Lake Michigan where the easterly winds from the lake breeze resulted in strong low-level wind shear. The axis of higher SRH did extend to the west along the warm front over northern Illinois as well. By 0100 UTC, the SRH values had increased (0-3 km SRH around 250 m^2 s^{-2} and 0-1 km SRH of 150-200 m^2 s^{-2}) over much of central and southern Wisconsin with the axis of highest SRH along the warm front. T03 showed that the 0-1 km helicity using the Bunkers et al. (2000) supercell motion estimate was statistically different between significantly tornadic supercells and nontornadic supercells. The large 0-1 km SRH in this case study is near the 50th percentile for significant tornadoes in T03. The SRH values based on observed storm motion are discussed later in this section.

The increase in low-level wind speed resulted in the northeastward movement of the warm front and its associated theta-e advection, with a large area of 1000-850 mb Q-vector convergence within the warm-air advection ahead of the low and cold front (Fig. 7b-d). The theta-e advection had resulted in a slight increase in MLCAPE (not shown) over central Wisconsin from 2200 UTC to 0100 UTC, despite the approach of sunset.

The 0000 UTC upper-air maps show the left exit region of a 300 mb jet streak and associated Q-vector convergence (Fig. 13a) remaining just north of the surface low, while appreciable 500 mb cyclonic vorticity advection and Q-vector convergence (Fig. 13b) is over southwestern Ontario and western Lake Superior, and also north of the surface low over west-central Wisconsin. When compared to the 1200 UTC maps (Fig. 3a-d), more of a displacement has occurred between the upper level Q-vector convergence and the surface low and cold front. This would explain why no further deepening of the low occurred after 2100 UTC (the low actually filled by 0.8 mb between 2100 UTC and 0300 UTC). Maddox and Doswell (1982) emphasized the importance of lower-tropospheric warm-air advection to convective events, especially in the less than "classic" synoptic scale settings. Overall this event was characterized by lower tropospheric warm-air advection, theta-e advection, and 1000-850 mb Q-vector convergence playing a key role in propagating the pressure falls and surface low eastward, and supplying moisture, instability, and synoptic-scale lift to the ongoing convection. The frontogenesis along the cold front and the supercell structures and gust fronts themselves provided the mesoscale and storm-scale lift to support continuing severe convection.

c. Gridpoint soundings

Proximity gridpoint soundings from the RUC were used to sample the near storm environment associated with the tornadic supercells. The soundings were generated for 0000, 0001, and 0200 UTC 24 June 2004. This coincided with the times that tornadic supercells approached and moved to a distance of 5 to 39 km from an ASOS or AWOS site (Table 1 and Fig. 2).

RUC proximity gridpoint soundings were generated at each of the six surface observation sites. The surface data in the model soundings were modified with the observed surface data (i.e., temperature, dewpoint, and wind) from the ASOS and AWOS sites. The time of surface observations coincided with the time of the generated proximity soundings with one exception – Sparta, Wisconsin (KCMY). Cool air from the outflow associated with an isolated cell modified the observation taken at the time of the sounding (0000 UTC 24 June). Therefore, the 2300 UTC 23 June surface observation was used to modify the model sounding since it was more representative of the near storm environment. Of interest, the isolated cell and its cool outflow did remain east and south of the tornadic supercell's path located northeast of KCMY. Finally, the ST1.5 was used for thermodynamic calculations while RUC sounding wind data were transferred to a locally developed program [available on line from the NOAA/National Weather Service Weather Forecast Office (WFO) Rapid City, SD, Web site at www.crh.noaa.gov/unr/?n=scm for calculations involving wind shear. Table 1 lists the severe weather parameters for each site. In following detail, the results of Table 1 are explored.

The MLBRN ranged from 2 to 12 which are partially in the supercell range of 10 to 40 determined by Weisman and Klemp (1982, 1984) through the use of a three-dimensional

Fig. 9(a-d). 0.5 Reflectivity from various WSR-88Ds over Wisconsin showing HP supercells.

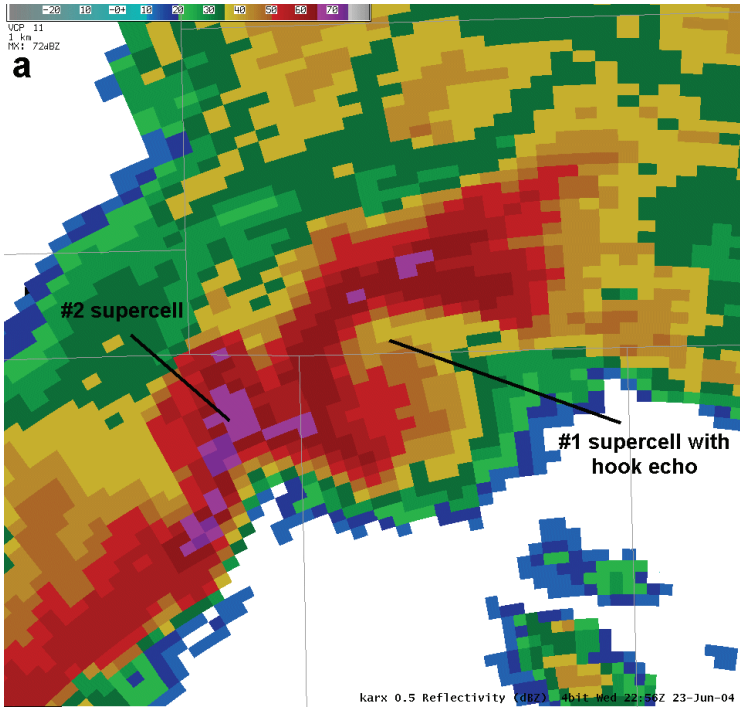

(a) Two conjoined HP supercells 92 km north of La Crosse (ARX) WSR-88D.

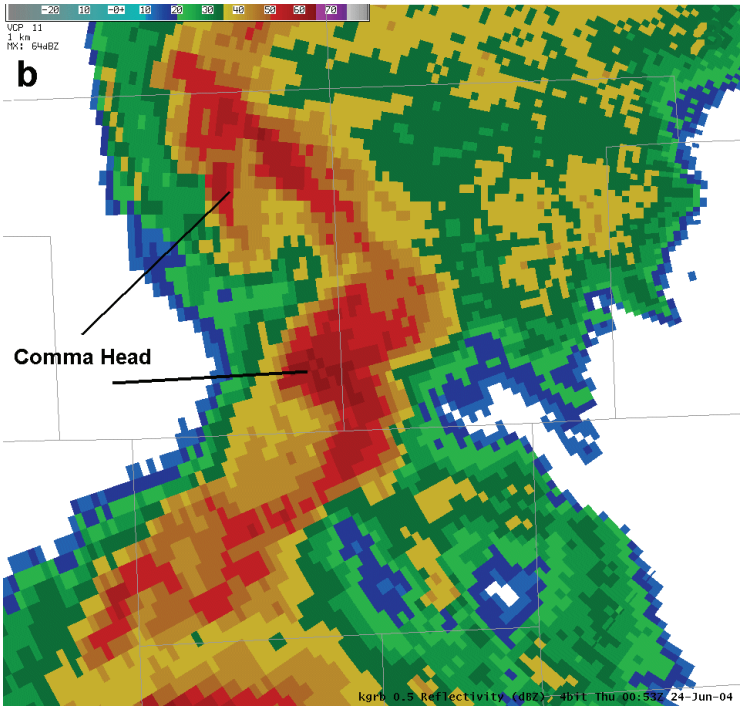

(b) Two tornadic HP supercells with comma head features 97 km west of Green Bay (GRB) WSR-88D.

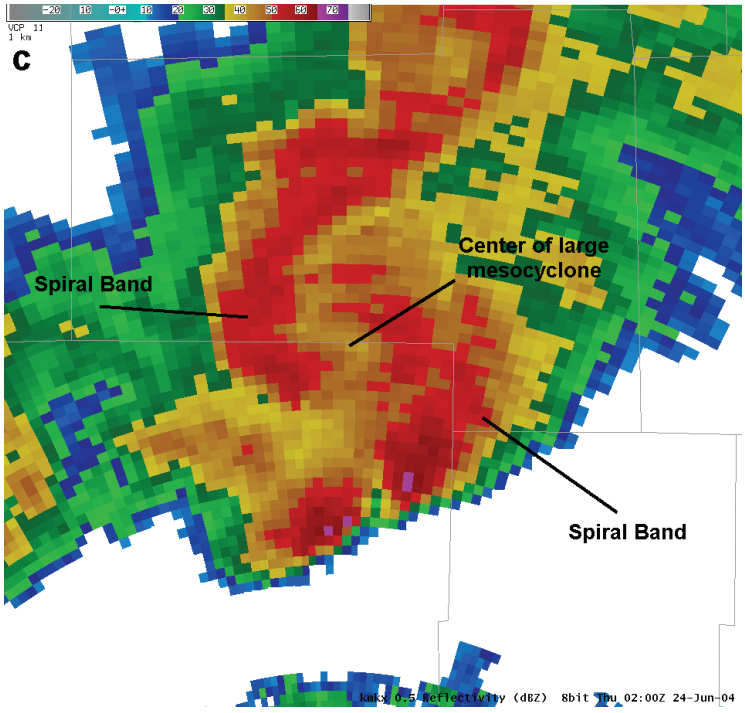

(c) Tornadic spiral-banded HP supercell 72 km north of Sullivan (MKX) WSR-88D.

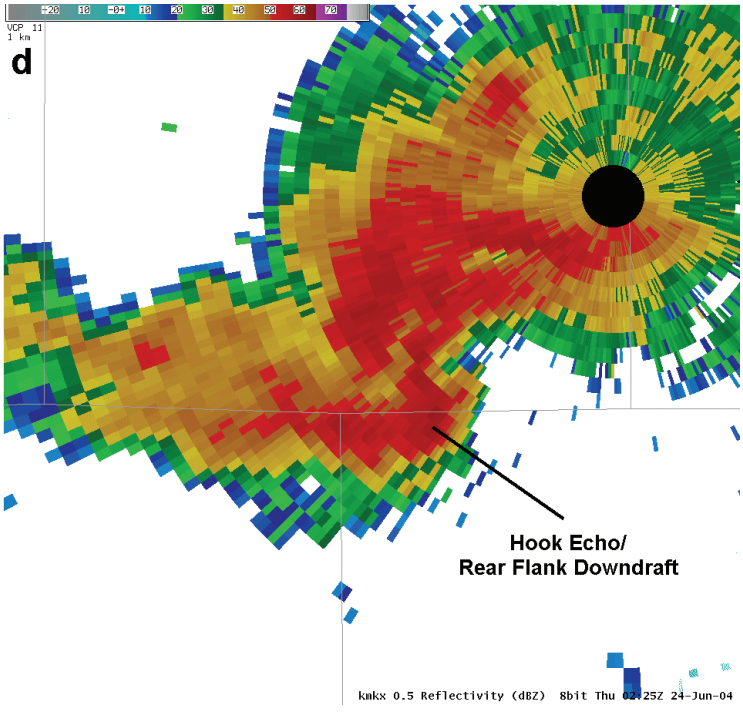

(d) Tornadic HP supercell with large RFD/hook echo 18 km southwest of Sullivan (MKX) WSR-88D.

cloud model. However, Johns et al. (1993) examined 242 proximity soundings of F2 and greater tornadoes and revealed that 47% occurred with BRNs less than 8 and nearly 79% less than 20. Riley and Colquhoun (1990) found that nearly 50% of their cases had BRN less than 21 for all ranges of the F-scale. Johns et al. (1993) noted that the majority of their tornadic supercells were associated with "complex multicellular convective structures", such as bow echoes, lines, clusters, and spiral bands. Moller et al. (1990, 1994) and Doswell et al. (1990) recognized many of these storms as HP supercells, with common characteristics of (1) rotation, (2) a "distinctive" (Forbes 1981) appearance on reflectivity despite being surrounded by other convection, and (3) containing a large amount of precipitation in the mesocyclone. Since HP supercells produced the majority of severe weather and tornadoes on 23 June 2004, further discussion is warranted.

More recent research on supercell type (Rasmussen and Straka 1998) focused on storm-relative (SR) upper flow. Rasmussen and Straka (1998) found SR upper flow greater than 30 m s^{-1} supported low precipitation (LP) supercells while SR flow of less than 12 m s^{-1} supported HP supercells. SR upper flow from 12-30 m s^{-1} and 0-3 km SRH less than 250 m^2 s^{-2} supported LP supercells while the same SR upper flow and 0-3 km SRH greater than 250 m^2 s^{-2} trended toward HP supercells. However, it was stressed that storm mergers and seeding from other storms may lead to HP supercells

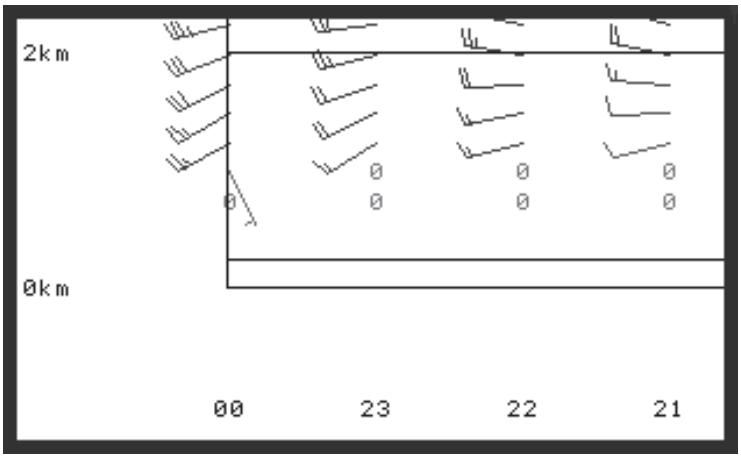

Fig. 10. Blue River, WI profiler data. Note increase in 0-2 km winds (kt) from 2100 UTC to 0000 UTC.

and that this process may dominate over SR upper flow.

On 23 June 2004 there were at least a half-dozen tornadic HP supercells that were embedded, surrounded, or merged with other convective cells very similar to the cases discussed by Johns et al. (1993) that had low BRN. The HP supercell type in this event was most likely a result from seeding due to the close spacing of the storms (Fig. 5c). The long-track HP supercell that produced six tornadoes had 10 km SR flow of 20 m s^{-1} and 0-3 km SRH of 260 m^2 s^{-2} (Fig. 14). This matches the SR upper flow and SRH that Rasmussen and Straka (1998) found for HP supercells. However, the long

RUC sounding	0100 UTC DLL	0100 UTC MSN	0100 UTC FLD	0000 UTC CMY	0000 UTC STE	0200 UTC GRB
Storm Motion	280° at 38 kt	284° at 40 kt	285° at 44 kt	282° at 45 kt	270° at 42 kt	280° at 36 kt
Location and time of tornado w.r.t. RUC sounding	39 km north at 0045 UTC 40 km northeast at 0100 UTC	12 km northwest at 0135 UTC	32 km southwest at 0145 UTC	24 km northeast at 2359 UTC	35 km southeast at 0050 UTC	5 km north at 0227 UTC
MLBRN	11	12	7	5	2	5
0-1 km Shear	8 m s^{-1}	10 m s^{-1}	11 m s^{-1}	9 m s^{-1}	7 m s^{-1}	6 m s^{-1}
MLLCL	.926 km	.985 km	.834 km	.995 km	1.206 km	.911 km
MLCAPE	1274 J kg^{-1}	1350 J kg^{-1}	903 J kg^{-1}	730 J kg^{-1}	303 J kg^{-1}	591 J kg^{-1}
0-3 km CAPE	121 J kg^{-1}	118 J kg^{-1}	108 J kg^{-1}	87 J kg^{-1}	94 J kg^{-1}	103 J kg^{-1}
MLLFC	1.301 km	1.285 km	1.246 km	1.402 km	1.403 km	1.452 km
MLCIN (negative)	21 J kg^{-1}	15 J kg^{-1}	22 J kg^{-1}	30 J kg^{-1}	14 J kg^{-1}	36 J kg^{-1}
0-3 km SRH	162 m^2 s^{-2}	204 m^2 s^{-2}	260 m^2 s^{-2}	174 m^2 s^{-2}	67 m^2 s^{-2}	147 m^2 s^{-2}
0-1 km SRH	106 m^2 s^{-2}	148 m^2 s^{-2}	175 m^2 s^{-2}	97 m^2 s^{-2}	82 m^2 s^{-2}	83 m^2 s^{-2}

Table 1. RUC Analysis Proximity Soundings and Severe Weather Parameters

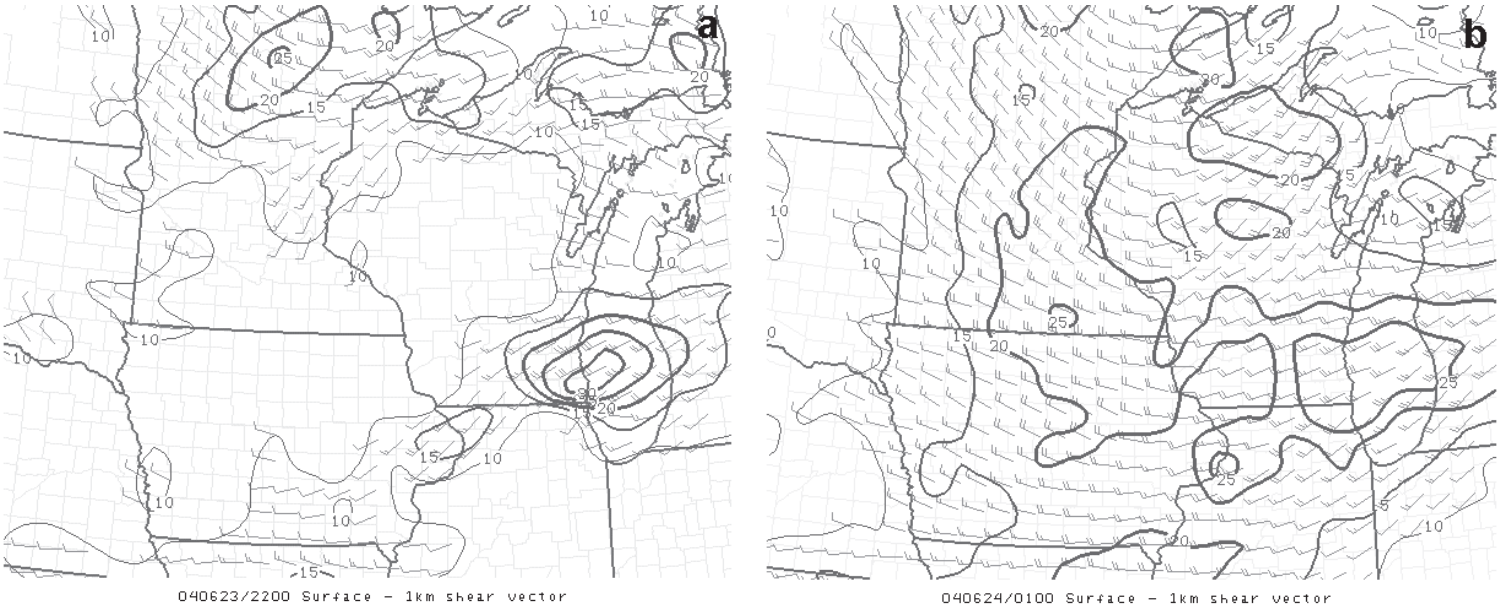

Fig. 11(a-b). SPC RUC-based Surface-1 km shear vector valid (a) 2200 UTC and (b) 0100 UTC.

track supercell intensified and clearly became an HP when a line of thunderstorms merged with it from the west. This HP supercell (Fig. 9c) produced 6 tornadoes including two F3-rated tornadoes and one F2-rated tornado. The F3-rated tornadoes occurred approximately 45 minutes after and 32 km southwest of the Fond du Lac, Wisconsin (KFLD) 0100 UTC RUC sounding (Fig. 14). The supercell lasted 3 hours and exhibited a large and strong persistent mesocyclone with a comma-head and spiral-banded reflectivity structure for the last two hours of its life cycle. Other HP supercells evolved into small-scale bow echoes with tornadogenesis occurring within the comma-head (Przybylinski 1995). One F0 tornado also developed along the leading edge of a bow structure south of the comma-head. This long-track HP supercell and the convective complex in general tracked east to southeast (~ 44 kt) along and ahead of the cold front but parallel to the slow northward moving warm front throughout the early evening (Fig. 4c-d).

The tornadic supercells traveling near the warm front are noteworthy since Markowski et al. (1998a) found that 70% of tornadoes in the Verification of the Origin of Rotation in Tornadoes Experiment (VORTEX-95) were near or within boundaries, usually from 10 km on the warm side to 30 km on the cool side. The process of tilting and stretching of horizontal vorticity associated with a boundary was believed to support low-level mesocyclogenesis. The tornado outbreak in this case study did fit the aforementioned research with tornadic HP supercells near a warm front that were surrounded, embedded, or merged with other convective cells, within a low BRN environment. The HP supercells also followed the two composite life cycles of HP supercells presented by Moller et al. (1990) in which a HP supercell transitions into a bow echo with a rotating comma head while the other becomes a cyclic HP supercell without transition into a bow echo.

The following severe weather parameters were also supportive of tornadic supercells.

The 0-1 km shear values in Table 1 hovered near the 25th percentile (lower rough threshold of 10 m s^{-1} and 8 m s^{-1}) in the significant tornado category in Craven et al. (2004) and T03 respectively. The ML lifting condensation level (MLLCL) in Table 1 fell mostly within the 25th to 75th percentile (low LCLs) for the significant tornado category of all three proximity sounding studies by Craven et al. (2004), Rasmussen and Blanchard (1998), and T03. LCLs are apparently critical to tornadogenesis since Markowski et al. (2002) observed warm, moist (low dewpoint depression air, thus low LCLs) RFD air containing some CAPE within tornadic storms versus nontornadic storms characterized by larger dewpoint depressions, and thus higher LCLs.

The 0-3 km CAPE values in Table 1 were large and fell mostly above the 75th percentile in the strong tornadic category in Rasmussen (2003). The ML level of free convection (MLLFC) values in Table 1 were near the 50th percentile (low LFC) in the strong tornadic category in Davies (2004) while the ML convective inhibition (MLCIN) values were within the 25th to 75th percentile. Values of large 0-3 km CAPE, low MLLFC, and low MLCIN on 23 June 2004 supported an environment of low-level parcel ascent and stretching that may have fostered a favorable environment for tornadogenesis (Davies 2004; Rasmussen 2003).

The 0-3 km SRH in Table 1 fell between the 25th and 75th percentiles in the significant tornado category for Rasmussen and Blanchard (1998), while Sparta (KCMY),

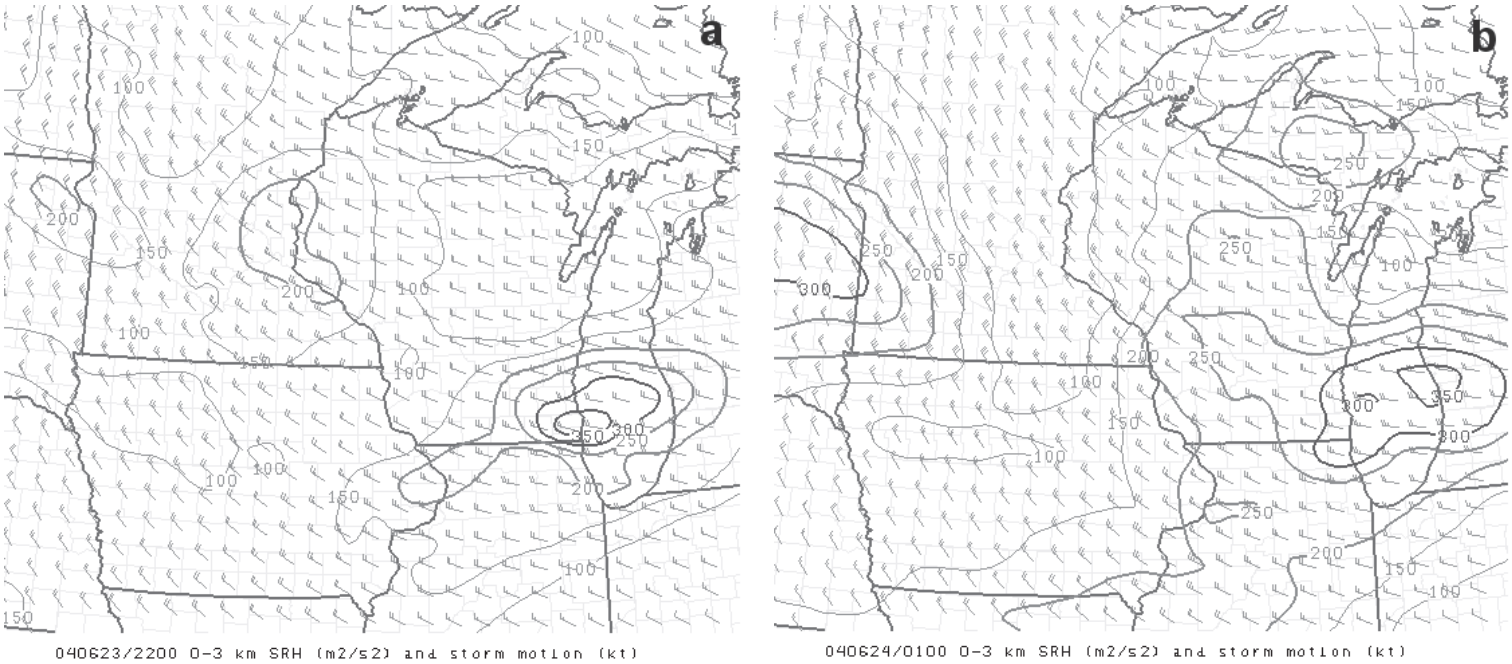

Fig. 12(a-d). SPC RUC-based 0-3 km SRH (a,b) and 0-1 km SRH (c,d) valid 2200 UTC and 0100 UTC respectively. SRH calculated using the Bunkers et al. (2000) supercell storm motion estimate.

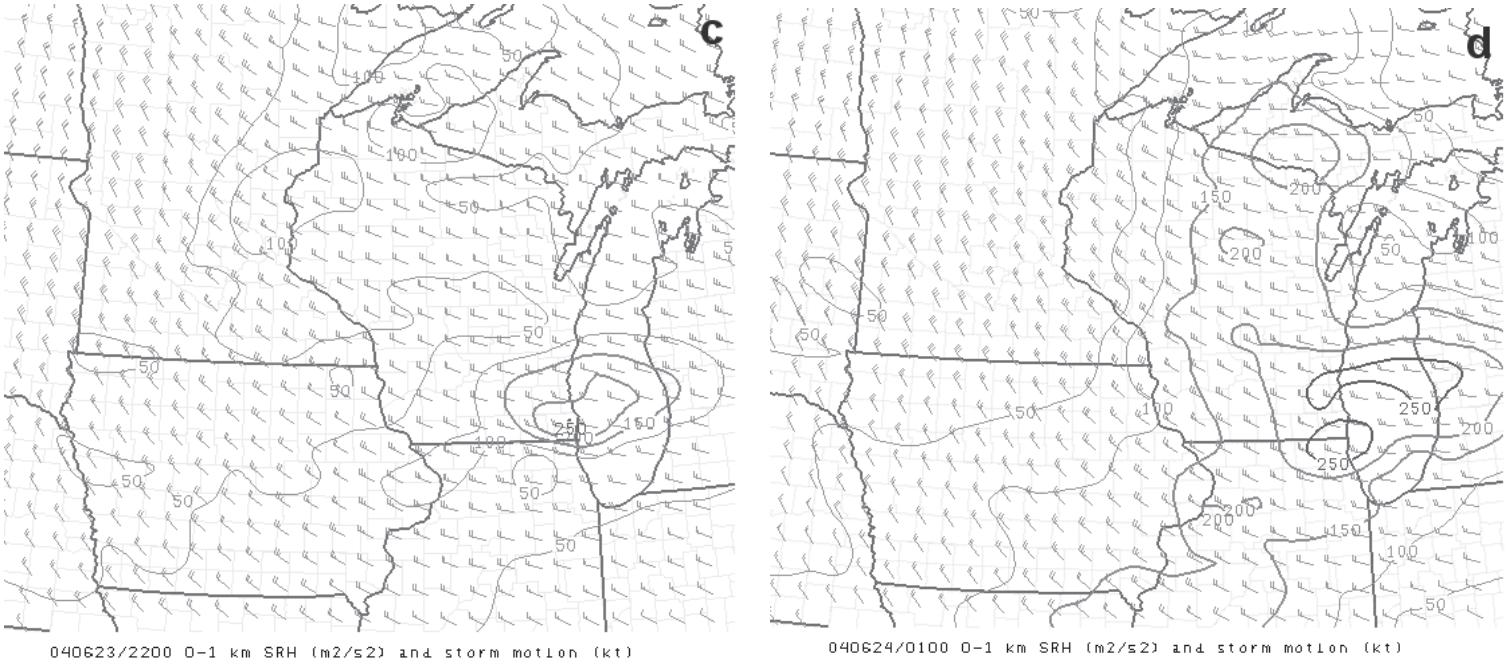

Madison (KMSN), and Fond du Lac, Wisconsin (KFLD) fell within the middle 50th percentile of T03. However, based on a large amount of overlap with other categories, 0-3 km SRH is best used as a supercell predictor (relative to the 0-1 km SRH). The 0-1 km SRH/wind shear was found by Markowski et al. (1998b) and Markowski et al. (2003) to be a strong indicator of significant tornadic supercells. Using over six thousand 0000 UTC soundings, Markowski et al. (1998b) found the 0-1 km SRH values for significant tornadic supercells averaged nearly 100 m^2 s^{-2} and accounted for nearly 53% of the SRH in the 0-3 km layer. Table 1 shows the 0-1 km SRH values ranged from 82 m^2 s^{-2} to 175 m^2 s^{-2}, and accounted for approximately 56-73% of the total 0-3 km SRH. In fact, the 0-1 km SRH was larger than the 0-3 km SRH at KSTE. The 0-1 km SRH fell within the 25th and 75th percentiles in Rasmussen (2003) while Baraboo (KDLL), Madison (KMSN) and Fond du Lac, Wisconsin (KFLD) fell within the middle 50th percentile of T03.

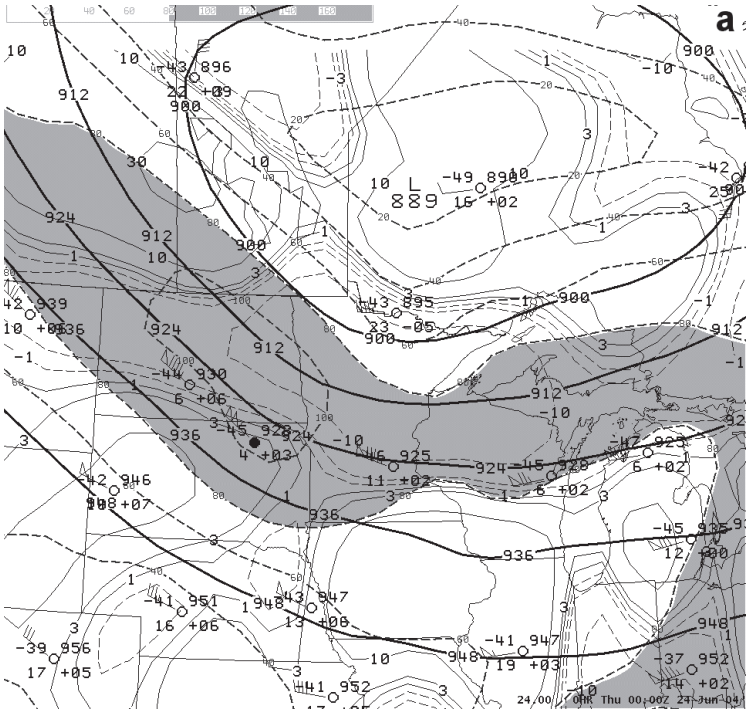

Fig. 13(a). Same as Fig. 3a except for 0000 UTC 24 June 2004.

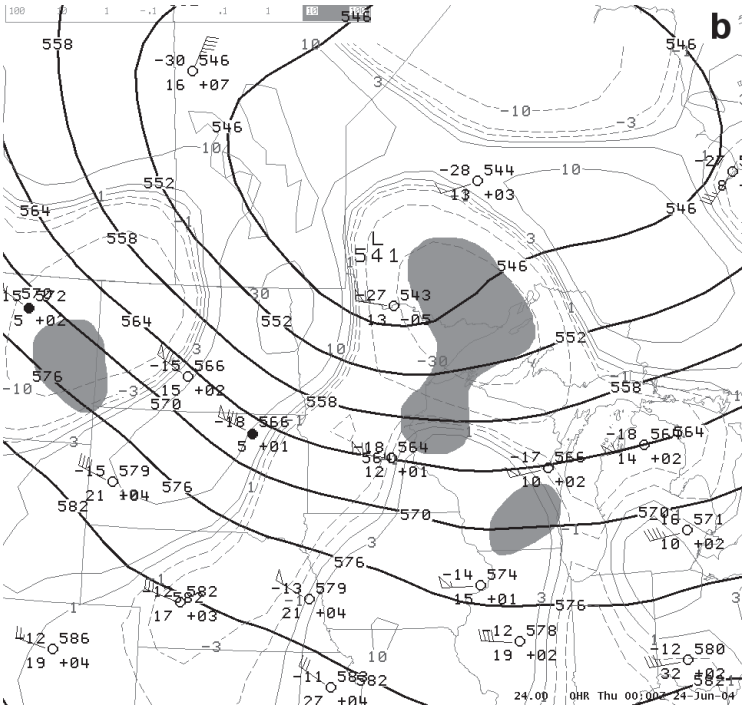

Fig. 13(b). Same as Fig. 3b except for 0000 UTC 24 June

Overall, the severe weather parameters from RUC proximity analysis soundings in Table 1 were supportive of tornadic supercells on 23 June 2004. The sounding for Stevens Point, Wisconsin (KSTE) was marginal for tornadic supercells, although there were two nearby weak tornadoes and an F2 tornado (HP with comma-head structure) 35 km to the southeast. The 0-3 km SRH value was low primarily because the storm motion (Table 1) was 270°, thereby plotted much closer to the hodograph, but the 0-1 km SRH value of 82 m^2 s^{-2} was respectable. The KFLD and KDLL proximity soundings were taken to represent the long-track HP supercell that was responsible for six tornadoes (three of which were strong). The strong tornadoes occurred closest to KFLD and the sounding revealed the lowest MLLCL and MLLFC and the highest low level wind shear (SRH and 0-1 km shear) compared to the remainder of the proximity soundings. Figure 14 is the hodograph for KFLD with observed storm motion plotted. The parameters for this particular HP supercell were in solid agreement with the strong tornadic supercell distributions of the various referenced authors in this paper. The 4-6 km SR flow of 24 kt and the 10 km SR flow of 39 kt were the median values in the strong tornado category for T03 and Rasmussen and Blanchard (1998) respectively.

4. Forecast Challenges

The NWS morning area forecast discussions and SPC outlooks for the morning of 23 June 2004 focused on the slow-moving cold front over Wisconsin (Fig. 3d). Convective initiation, aided by a weak shortwave trough, and possible severe weather ("slight risk" issued by SPC) were expected in the vicinity of the front by afternoon from Lower Michigan through central and southern Wisconsin into eastern Iowa. The discussions and outlooks identified a sufficient amount of moisture, CAPE, lift, and wind shear for damaging winds, large hail, and isolated tornadoes. The Northern Plains system was treated separately and with a slower forecast progression than what was observed.

The afternoon area forecast discussions and SPC outlooks continued to keep the two systems separate. The lack of moisture and CAPE across Wisconsin in the early afternoon, and the expected northward displacement of the most focused upper-level dynamics (Fig. 13a-b) contributed to lower confidence of severe convective potential among the local NWS forecast offices. The area forecast discussions mentioned little of the weak but developing surface low and isallobaric couplet that was occurring over Minnesota at the time. The slight risk was continued by the SPC and then upgraded to moderate risk by 0036 UTC 24 June 2004.

The 1200 UTC 23 June 2004 Eta forecasted a reasonably well depiction of the event. The surface low and northward moving warm front were resolved by the model, but were slightly slower with the progression compared to the observed surface maps. The 1200 UTC Eta correctly forecasted 0-3 km SRH above 200 m^2 s^{-2} and accurately placed the north to south CAPE gradient over central and southern Wisconsin. The previous run from 0000 UTC 23 June 2004

Eta was farther north than the 1200 UTC run and positioned the morning cold front to the east and south by late afternoon and evening. With no indication of the cold front possibly reversing and moving to the north as a warm front, the warm-air advection and 0-3 km SRH were consequently weaker. This case clearly was not "synoptically evident" (Doswell et al. 1993) on the Eta or the current analyses throughout the day due to the weak surface low, strong upper-level dynamics (Fig. 13a-b) north of the outbreak area and marginal CAPE over central Wisconsin. In addition, the incorrect depiction of the event by the 0000 UTC 23 June 2004 Eta model led to difficulty in determining how significant and widespread the severe weather would be.

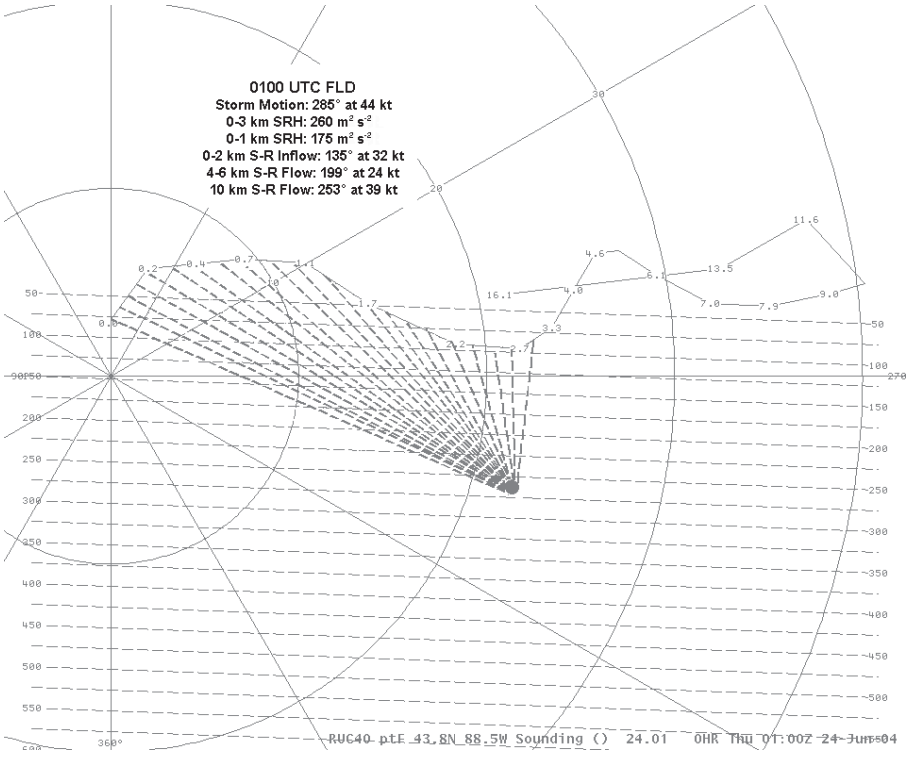

Fig. 14. 0100 UTC KFLD hodograph with observed storm motion. Hodograph in m s^{-1} .

5. Summary and Conclusions

On 23 June 2004, Wisconsin's fifth largest tornado outbreak occurred during the late afternoon and early evening hours. The parent deep moist convection was comprised of complex storm structures, bow echoes, and HP supercells. The event was characterized by a fast propagating isallobaric couplet and surface low with a 100 kt 300-mb jet streak, and a pre-existing front that lifted northward as a warm front. Low-level tropospheric warm-air advection, positive theta-e advection, frontogenesis, and convergence along the fronts and surface troughs appeared to be the catalyst for synoptic scale and mesoscale lift. In addition, an increase in low-level wind shear late in the day was a key ingredient in the development of tornadic supercells. The RUC proximity soundings were characterized by low BRN, low MLLCL, low MLLFC, low MLCIN, high 0-3 km CAPE, high SRH, and high 0-1 km shear. The values of these parameters, were favorable for tornadic supercells by late afternoon and evening.

This study suggests factors that can assist forecasters in anticipating high impact severe weather events when the numerical model predictions suggest otherwise. These factors include a severe weather conceptual knowledge base, a diligent "weather watch", and the utilization of progressive tools (e.g., mesoscale models) that add value beyond well established forecast practices.

Conceptual thinking based upon empirical forecast experience, informal case studies, and findings from published research provides the foundation from which forecasters can then employ a diligent "weather watch" in a skilled and efficient manner. Knowing what to look for and the implications of what is found on all scales (i.e., synoptic, meso, and storm) should present better opportunities to more accurately and in a more timely fashion anticipate convection initiation, the predominant convective mode, significant changes to the convective mode and the resulting weather impacts. Finally, high resolution mesoscale models configured to address critical forecast issues provide the means to evaluate changes to the pre-storm and near-storm environments both in real-time or as a valuable post-analysis research tool.

Author

Mark Gehring is a Journeyman Forecaster with the National Weather Service Weather Forecast Office (WFO) in Sullivan, Wisconsin. He also has worked as a Meteorologist Intern at the Elko, Nevada WFO office before coming to the Sullivan office in 2000. He earned his B.S. in Geosciences from the University of Wisconsin-Milwaukee in 1997 and earned his M.S. in Geosciences from the University of Wisconsin-Milwaukee in 1999. His meteorological interests include severe convection, fire weather, and flash flooding. He can be contacted at Mark Gehring, National Weather Service, N3533 Hardscrabble Road, Dousman, WI 53118; E-mail: Mark.G.Gehring@noaa.gov.

Acknowledgments

The author would like to thank Bill Borghoff for his time and effort in drafting the figures for this paper. The author benefited from discussions with the entire staff at NWS Milwaukee/Sullivan, including Bill Borghoff and Alex Lamers. John Eise and Alex Lamers provided much of the data used in this manuscript. The author thanks Matthew Bunkers for providing a locally developed program used for wind shear calculations. Lastly, the author thanks Kim Licitar for his help and expertise in maintaining the software used in this study.

References

Benjamin, S. G., D. Dévényi, S. S. Weygandt, K. J. Brundage, J. M. Brown, G. A. Grell, D. Kim, B. E. Schwartz, T. G. Smirnova, T. L. Smith, and G. S. Manikin, 2004: An hourly assimilation–forecast cycle: The RUC. *Mon. Wea. Rev.,* 132, 495–518.

Bothwell, P.D., J.A. Hart, and R.L. Thompson, 2002: An integrated three-dimensional objective analysis scheme in use at the Storm Prediction Center. Preprints, *21st Conference on Severe Local Storms,* San Antonio, TX, Amer. Meteor. Soc., J117-J120.

Bunkers, M.J., and M. Magsig, X. Yu, 2005: Sounding Toolkit Version 1.5. NWS AWIPS Local Application.

_____, B.A. Klimowski, J.W. Zeitler, R.L. Thompson, and M.L. Weisman, 2000: Predicting supercell motion using a new hodograph technique. *Wea. Forecasting*, 15, 61-79.

Craven, J.P., and Harold E. Brooks, 2004: Baseline climatology of sounding derived parameters associated with deep, moist convection. *Natl. Wea. Dig.,* 28, 13-24.

_____, R.E. Jewell, and H.E. Brooks, 2002: Comparison between observed convective cloud-base heights and lifting condensation level for two different lifted parcels. *Wea. Forecasting*, 17, 885-890.

Davies, J. M., 2004: Estimations of CIN and LFC associated with tornadic and nontornadic supercells. *Wea. Forecasting,* 19, 714-726.

Davies-Jones, R.P., D. Burgess, and M. Foster, 1990: Test of helicity as a tornado forecast parameter. Preprints, *16th Conference on Severe Local Storms,* Kananaskis Park, Alberta, Canada, Amer. Meteor. Soc., 588-592.

Doswell, C.A. III, 1987: The distinction between large-scale and mesoscale contribution to severe convection: A case study example. *Wea. Forecasting,* 2, 3-16.

_____, and E.N. Rasmussen, 1994: The effect of neglecting the virtual temperature correction on CAPE calculations. *Wea. Forecasting,* 9, 625-629.

_____, A.R. Moller, and R. Przybylinski, 1990: A unified set of conceptual models for variations on the supercell theme. Preprints, *16th Conference on Severe Local Storms,* Kananaskis Park, Alberta, Canada, Amer. Meteor. Soc., 40-45.

_____, S.J. Weiss, and R.H. Johns, 1993: Tornado forecasting--A review. *The Tornado: Its Structure, Dynamics, Prediction, and Hazaards, Geophys. Monogr.,* No. 79, Amer. Geophys. Union, 557-571.

_____, R. Edwards, R.L. Thompson, J.A. Hart, and K.C. Crosbie, 2006: A simple and flexible method for ranking severe weather events. *Wea. Forecasting,* 21, 939-951.

Forbes, G.S., 1981: On the reliability of hook echoes as tornado indicators. *Mon. Wea. Rev.,* 109, 1457-1466.

Fujita, T.T., 1971: Proposed characterization of tornadoes and hurricanes by area and intensity. Satellite and Mesometeorology Research Paper No. 91, Dept. of Geophysical Sciences, University of Chicago, 42 pp.

_____, 1978: Manual of downburst identification for project NIMROD. Satellite and Mesometeorology Research Paper No. 156, Dept. of Geophysical Sciences, University of Chicago, 104 pp.

Galway, J.G., 1977: Some climatological aspects of tornado outbreaks. *Mon. Wea. Rev.,* 105, 477-484.

Johns, R.H., 1982: A synoptic climatology of northwest flow severe weather outbreaks. Part I: Nature and significance. *Mon. Wea. Rev.,* 110, 1653-1663.

_____, 1984: A synoptic climatology of northwest flow severe weather outbreaks. Part II: Meteorological parameters and synoptic patterns. *Mon. Wea. Rev.,* 112, 449-464.

_____, and C. A. Doswell III, 1992: Severe local storms forecasting. *Wea. Forecasting*, 7, 588-612.

_____, J.M. Davies, and P.W. Leftwich, 1993: Some wind and instability parameters associated with strong and violent tornadoes. 2. Variations in the combinations of wind and instability parameters. *The Tornado: Its Structure, Dynamics, Prediction, and Hazards, Geophys. Monogr.,* No. 79, Amer. Geophys. Union, 583-590.

Maddox, R.A., and C.A. Doswell III, 1982: An examination of jet stream configurations, 500 mb vorticity advection and low-level thermal advection patterns during extended periods of intense convection. *Mon. Wea. Rev*., 110, 184-197.

Magsig, M. A., T. Decker, and N. M. Said, 2006: Builds five and six of NOAA's NWS weather event simulator. Preprints, *22nd International Conference on Interactive Information and Processing Systems (IIPS)*, Atlanta, GA, Amer. Meteor. Soc., CD-ROM, 7.7.

Markowski, P.M., E.N. Rasmussen, and J.M. Straka, 1998a: The occurrence of tornadoes in supercells interacting with boundaries during VORTEX-95. *Wea. Forecasting,* 13, 852-859.

_____, J.M. Straka, and E.N. Rasmussen, 1998b: A preliminary investigation of the importance of helicity 'location' in the hodograph. Preprints, *19th Conference on Severe Local Storms*, Minneapolis, MN, Amer. Meteor. Soc., 230-233.

_____, J.M. Straka, and E.N. Rasmussen, 2002: Direct surface thermodynamic observations within the rear-flank downdrafts of nontornadic and tornadic supercells. *Mon. Wea. Rev.*, 130, 1692-1721.

_____, C. Hannon, J. Frame, E. Lancaster, A. Pietrycha, R. Edwards, and R. Thompson, 2003: Characteristics of vertical wind profiles near supercells obtained from the Rapid Update Cycle. *Wea. Forecasting*, 18, 1262-1272.

Moller, A.R., C.A. Doswell III, and R. Przybylinski, 1990: High precipitation supercells: A conceptual model and documentation. Preprints, *16th Conference on Severe Local Storms,* Kananaskis Park, Alberta, Canada, Amer. Meteor. Soc., 52-57.

_____, _____, M.P. Foster, and G.R. Woodall, 1994: The operational recognition of supercell thunderstorm environments and storm structure. *Wea. Forecasting,* 9, 327-347.

Przybylinski, R.W., 1995: The bow echo: Observations, numerical simulations, and severe weather detection methods. *Wea. Forecasting*, 10, 203-217.

Rasmussen, E.N., 2003: Refined supercell and tornado forecast parameters. *Wea. Forecasting,* 18, 530-535.

_____, and D.O. Blanchard, 1998: A baseline climatology of sounding-derived supercell and tornado forecast parameters. *Wea. Forecasting*, 13, 1148-1164.

_____, and J.M. Straka, 1998: Variations in supercell morphology. Part I: Observations of the role of upper-level storm-relative flow. *Mon. Wea. Rev.,* 126, 2406-2421.

Riley, P.A., and J.R. Colquhoun, 1990: Thermodynamic and wind related variables in the environment of United States tornadoes and their relationship to tornado intensity. Preprints, *16th Conference on Severe Local Storms*, Kananaskis Park, Alberta, Canada, Amer. Meteor. Soc., 599-602.

Thompson, R.L., 1998: Eta Model storm-relative winds associated with tornadic and nontornadic supercells. *Wea. Forecasting*, 13, 125-137.

_____, R. Edwards, J. A. Hart, K. L. Elmore, and P. Markowski, 2003: Close proximity soundings within supercell environments obtained from the Rapid Update Cycle. *Wea. Forecasting*, 18, 1243-1261.

Weisman, M.L., and J.B. Klemp, 1982: The dependence of numerically simulated convective storms on wind shear and buoyancy. *Mon. Wea. Rev.*, 110, 504-520.

_____, and _____, 1984: The structure and classification of numerically simulated convective storms in directionally varying wind shears. *Mon. Wea. Rev.*, 112, 2479-2498.